Radiomic Analysis for Pretreatment Prediction of Recurrence After Radiotherapy in Locally Advanced Cervical Cancer

Daisuke Kawahara (daika99@hiroshima-u.ac.jp)
Hiroshima University
Ikuno Nishibuchi
Hiroshima University
Masashi Kawamura
Hiroshima University
Takahito Yoshida
Hiroshima University
Iemasa Koh
Hiroshima University
Katsuyuki Tomono
Hiroshima University
Masaki Sekine
Hiroshima University
Haruko Takahashi
Hiroshima University
Yutaka Kikuchi
Hiroshima University
Yoshiki Kudo
Hiroshima University
Yasushi Nagata
Hiroshima University

Research Article

Keywords: Radiotherapy, machine learning, cervix cancer

Posted Date: January 31st, 2022

DOI: https://doi.org/10.21203/rs.3.rs-1198222/v1

Version of Record: A version of this preprint was published at International Journal of Radiation Oncology*Biology*Physics on November 1st, 2021. See the published version at https://doi.org/10.1016/j.ijrobp.2021.07.477.

Abstract

Objective To predict the recurrence of advanced cervical cancer patients treated with radiotherapy from radiomics features on pre-treatment T1- and T2-weighted MRI images.

Methods A total of 90 patients were split into two sets: 67 patients for model training and 23 patients for model testing. The patient outcome was classified into two groups; patients with a recurrence (group I) and without a recurrence (group II). The predictors were selected using the least absolute shrinkage and selection operator (LASSO) regression. The machine learning for the predictive models was sued neural network classifiers. The accuracy, sensitivity, specificity, and the area under the curve (AUC) from the receiver operating characteristic were evaluated.

Results By the LASSO analysis, we found 25 radiomics features from the T1-weighted MRI image and 4 radiomics features from the T2-weighted MRI image. The accuracy of the prediction model was highest with the combination of T1- and T2-weighted MRI images. The model performances with T1-weighted MRI image and T2-weighted MRI image were 86.4% and 89.4% of accuracy, 74.9% and 38.1% of sensitivity, 81.8% and 72.2% of specificity, and 0.89 and 0.69 of AUC. The model performance was improved with the combination of T1- and T2-weighted MRI images, which was 93.1% of accuracy, 81.6% of sensitivity, 88.7% of specificity, and 0.94 of AUC.

Conclusions The radiomics analysis with T1- and T2-weighted MRI images could highly predict the recurrence of the cervix cancer after radiotherapy. The variation of the distribution and the difference of the pixel number at the peripheral and the center were important predictors.

Key Points

- • A MRI-based radiomics model for the prediction of the recurrence of advanced cervical cancer patients treated with radiotherapy was proposed.
- • The accuracy of the prediction model was highest with the combination of T1- and T2-weighted MRI images.
- • The model performance was improved with the combination of T1- and T2-weighted MRI images, which was 93.1% of accuracy, 81.6% of sensitivity, 88.7% of specificity, and 0.94 of AUC.

Introduction

Cervical cancer is one of the most frequent malignant tumors in worldwide females [1]. Definitive radiotherapy is the mainstream of cervical squamous cell carcinoma for both early-stage and advanced cases. In early-stage, the treatment outcomes of radiotherapy and surgery are comparable. For locally advanced unresectable cervix cancer, concurrent chemoradiotherapy (CCRT) is the standard treatment. However, Jemal et al reported that one-third of patients would experience recurrence [2]. After primary therapy, tumor recurrence is frequently not detected for several months. It is a major challenge to predict the treatment response and the long-term outcome presents for a precise personalized care. In clinical, patients can take the treatment such as additional chemotherapy and dose escalation in time for those patients by predicting reliable biomarkers that can early identify the high-risk recurrence patients.

A medical image such as magnetic resonance imaging (MRI) and computed tomography is essential in the staging of patients and guiding treatment decisions. For cervical cancer patients, the MRI provides high soft-tissue contrast and functional information, which plays a key role in the assessment of the reference standard for the pre-therapeutic [3].

Radiomics analysis provides high-dimensional data such as tumor homogeneity and heterogeneity that cannot be identified by general visual evaluation using texture analysis in addition to the shape and volume [4, 5]. Texture analysis can evaluate the position of the pixels and gray-level intensity within an image using a variety of mathematical methods.

Radiomics can classify the stage or histology of the tumor through the prediction of responses to chemotherapy [6] or radiotherapy [7].

Reuze et al reported that the PET texture analysis could predict the recurrence for locally advanced cervical cancer treated by brachytherapy and chemoradiation than SUVmax [8]. Meng et al evaluated a useful of texture features extracted from T2-weighted MRI image and apparent diffusion coefficient (ADC) maps for prediction of recurrence for advanced cervical cancer patients treated with concurrent chemoradiotherapy [9]. The prediction model with MRI image improved the accuracy of the prediction than that with PET image. On the other hand, the region of interests (ROIs) were drawn on each slice covering the whole tumor. Xie et al showed usability of a sub-region-based radiomics analysis in which the ROI was divided into sub-regions based on the local entropy and cluster of CT values [10]. It suggests that the number of radiomics features could be increased by adding the ROI and it could improve the accuracy of the prediction.

The current study proposed the prediction model of the recurrence for cervical cancer patients treated e radiomics features using radiomics features extracted from the extended and shrink-uterus regions on pre-treatment T1- and T2-weighted MRI images.

Materials And Methods

A) Patients

Eighty-nine cervical squamous cell carcinoma patients who were treated with external beam radiotherapy (EBRT) followed by intracavitary brachytherapy (ICBT) at our institution from 2003 to 2015 were reviewed. All patients provided written informed consent for treatment. The patients and tumor characteristics are presented in Table 1. Among the M1 cases, patients with para-aortic lymph node (PAN) metastasis were included. Hiroshima University Certified Review Board approved this retrospective study (E-1656). The need for informed consent was waived owing to the retrospective nature of the study. The methods in the current study were performed according to relevant regulations and guidelines.

Table 1
Patient and tumor characteristics

Age (years)	Median (range)	63 (30-85)
PS	0	71
	1	14
	2	4
	3	0
Histology	Squamous	89
T factor (UICC-8th)	1a	1
	1b	8
	2a	1
	2b	37
	3a	0
	3b	36
	4a	6
N factor	0	43
	1	46
M factor	0	76
	1	13

B) Image Acquisition

MRI images were scanned with three 1.5 T MRI imaging units (Integenia Ambition, Philips; Siemens Healthcare Magnetom Avanto; Signa Excite, GE Healthcare), with a pelvic array coil for the pelvic scans. All patients were scanned using the same MR sequence, including axial T1-weighted fast spin-echo (FSE), and axial T2-weighted FSE. The patients who scanned only T1- or T2-weighted FSE with fat saturation were eliminated in the analysis. Images from 89 patients were retrospectively analyzed under an institutional-review-board-approved study.

C) Treatment

Radiotherapy

One patient was treated with ICBT alone, and 88 patients were treated with a combination of EBRT and ICBT. Three-dimensional radiotherapy planning was performed for all the patients who received EBRT using an X-ray beam (6–18 MV). Patients without PAN metastasis received whole pelvis irradiation (WPI) and patients with PAN metastasis received extended-field irradiation. Center shielding (CS) was used in 67 patients and boost irradiation for lymph node or parametrium regions was performed in 36 patients. The indication and dose of CS and boost irradiation were ultimately determined by the radiation oncologist based on the initial tumor size and therapeutic effect of WPI. The median EBRT dose was 50 Gy/25 fractions (range 28-66 Gy). Image-guided brachytherapy (IGBT) was performed in 20 patients. The prescribed dose of ICBT was 6 Gy to point A (a point 2 cm cranial from the external cervical os and 2 cm lateral from the

tandem) in two-dimensional treatment planning and to D90 (minimum dose to the 90%) of high-risk clinical target volume (the residual tumor at the time of ICBT and the whole uterine cervix) in IGBT. The fractions of ICBT depended on CS dose and the median ICBT dose was 18 Gy/3 fractions (range 6-30 Gy/1-5 fractions). The median overall treatment time was 44 days (range 30-58 days). The most common treatment schedule was as follows: whole pelvis irradiation 40 Gy/20 fractions, CS 10 Gy/5 fractions, and ICBT 18 Gy/3 fractions.

Chemotherapy

Sixty-eight patients received concurrent chemotherapy. According to our hospital's protocol and the physician's judgment, the selection of chemotherapeutic regimen and reduction of chemotherapeutic dosages were determined. The regimens of the chemotherapeutic were as follows: weekly cisplatin in 33 patients, weekly nedaplatin in 21 patients, intraarterial chemotherapy in 10 patients, and others in four patients.

F) Radiomics Analysis

The process acquisition of the MRI images to prediction model is shown in Fig. 1. The proposed radiomics model was designed as a Transparent Reporting of a Prediction Model for Individual Prognosis or Diagnosis (TRIPOD) type 2a [11]. The T1- and T2-weighted The MRI images were transferred to a medical image computing tool (3D Slicer, www.slicer.org) [12]. Fig. 2 shows the example of the segmentation. Uterus included the primary tumor was defined as CTV was manually segmented on the axial T1- and T2-weighted MRI images. The segmentation was performed by one or two radiation oncologists, including one expert radiation oncologist Then, the extended-CTVs were generated by adding 5 mm, 10 mm, and 20 mm margins from the CTV, which were defined as eCTV5, eCTV10, and eCTV20. Moreover, shrink-CTVs were generated by adding 5 mm and 10 mm margins from the CTV, which were defined as sCTV5 and sCTV10. The radiomics features were extracted with an open-source package in Python, Pyradiomics software [13]. A detailed list of the radiomics features is shown in Table 2 and Table 3.

Table 2
Feature type and associated features

Feature type	Morphology -based	First order-based	Texture-based				
Methods	Shape	Histogram	GLCM	GLSZM	GLRLM	NGTDM	GLDM
Feature name	Maximum 3D diameter	Interquartile range	Joint average	Gray level variance	Short run low gray level emphasis	Coarseness	Gray level variance
	Maximum 2D diameter slice	Skewness	Sum average	Zone variance	Gray level variance	Complexity	High gray level emphasis
	Sphericity	Uniformity	Joint entropy	Gray level non uniformity normalized	Low gray level run emphasis	Strength	Dependence entropy
	Minor axis	Median	Cluster shade	Size zone non uniformity normalized	Gray level non uniformity normalized	Contrast	Dependence non uniformity
	Elongation	Energy	Maximum probability	Size zone non uniformity	Run variance	Busyness	Gray level non uniformity
	Surface volume ratio	Robust mean absolute deviation	Idmn	Gray level non uniformity	Gray level non uniformity		Small dependence emphasis
	Volume	Mean absolute deviation	Joint energy	Large area emphasis	Long run emphasis		Small dependence high gray level emphasis
	Major axis	Total energy	Contrast	Small Area high gray level emphasis	Short Run high gray level emphasis		Dependence non uniformity normalized
	Surface area	Maximum	Difference entropy	Zone percentage	Run length non uniformity		Large dependence emphasis
	Flatness	Root mean squared	Inverse variance	Large area low gray level emphasis	Short run emphasis		Large dependence low gray level emphasis
	Least axis	90 percentile	Difference variance	Large area high gray level emphasis	Long run high gray level emphasis		Dependence variance
	Maximum 2D diameter column	Minimum	Idn	High gray level zone emphasis	Run percentage		Large dependence high gray level emphasis

Feature type	Morphology -based	First order-based	Texture-based			
	Maximum 2D diameter row	Entropy	Idm	Small area emphasis	Long run low gray level emphasis	Small dependence low gray level emphasis
		Range	Correlation	Low gray level zone emphasis	Run entropy	Low gray level emphasis
		Variance	Autocorrelation	Zone entropy	High gray level run emphasis	
		10 percentile	Sum entropy	Small area low gray level emphasis	Run length non uniformity normalized	
		Kurtosis	Sum squares			
		Mean	Cluster prominence			
			Imc2			
			Imc1			
			MCC			
			Difference average			
			Id			
			Cluster tendency			

Table 3
Feature associated with the imaging filters

Feature type	Wavelet-based
Methods	First-order statistic and texture of wavelet decomposition. Decomposition levels: LLL, LLH, LHL, LHH, HLL, HLH, HHL, HHH.
Feature name	First-order features
	GLCM features
	GLSZM features
	GLRLM features
	NGTDM features
	GLDM features

We extracted 13 shape radiomics features, 21 first-order radiomics features, 50 quantitative radiomics features, and 93 texture radiomics features. Additionally, the radiomics features were extracted from the wavelet filters which has high-pass

and low-pass filters. The wavelet filter was decomposed in x, y, and z direction. A total of 837 radiomics features were extracted for each segmentation.

G) Prediction Model

In this study, all loco-regional recurrence and distant metastasis after RT were regarded as recurrence and examined the prediction model for recurrence. The clinical patient data were updated in May 2020 and the median follow-up time was 59 months (range, 1–160 months). At the time of the last follow-up, recurrence was observed in 30 of 89 patients.

The least absolute shrinkage and selection operator (LASSO) regression model was used with MATLAB code to prevent overfitting [14, 15]. The most significant predictive features were selected with the LASSO regression which reduces the dimension from among all the candidate features in the training dataset.

We classified recurrence patients and non-recurrence patients with ML classifiers. The recurrence and non-recurrence patients were labeled as 1 and 0, respectively. The machine learning (ML) classifiers used a neural network (NN) with rectified linear unit activation and 10 hidden layers. All patients were randomly divided into a training set (49 patients), a validation set (14 patients), and a testing set (26 patients). The prediction model was constructed with the five-fold cross-validation method, as shown in Fig. 3. The predictive performance was evaluated using the area under the curve (AUC) from the receiver operator characteristic (ROC) curve, accuracy, sensitivity, and specificity.

Results

A total of 5022 features were extracted from T1-weighted MRI images and the T2-weighted MRI images, respectively. T1-weighted MRI image was finally reduced to 25 features and the T2-weighted MRI image was finally reduced to 4 features with the LASSO regression model, as shown in Fig. 4 and Table 4. The following features were extracted from the T1-weighted MRI image: 1 feature from the CTV, 2 features from the eCTV5, 7 features from the eCTV20, 5 features from the sCTV5, 10 features from the sCTV10. From the T2-weighted MRI image, 1 feature from the CTV, 1 feature from the eCTV20, 1 feature from the sCTV20, and 1 feature from the sCTV10 were extracted. Most of the features with the wavelet filter were extracted. The T1-weighted MRI image had a large number of features used for the prediction model than the T2-weighted MRI image. The features of the low-pixel number at the center region of the uterus for the T1-weighted MRI image mean the low blood flow. From the shrink-CTV (sCTV) analysis, the radiomics feature of a lower pixel number and a high conformality was selected from the T1- and T2-weighted MRI images. The area of the low pixel number was larger and the conformality was larger with the T1-weighted MRI image for the recurrence group. In the while, the mean value of low pixel number was smaller and the low pixel number with T2-weighted MRI image for the recurrence group. From the extended-CTV, the features that showed a nonuniformity, asymmetric distribution of the pixel values, and a larger volume with the high pixel number were selected.

Table 4
Selected the features by LASSO Cox regression.

ROI	Filter	Feature list	
T1-weighted MRI image			
CTV	wavelet-LLH	Firstorder	Skewness
eCTV5	wavelet-HLL	GLDM	LargeDependenceHighGrayLevelEmphasis
eCTV5	wavelet-HLH	GLCM	Correlation
eCTV20	original	Shape	SurfaceVolumeRatio
eCTV20	original	GLCM	MCC
eCTV20	wavelet-LLH	GLSZM	GrayLevelNonUniformity
eCTV20	wavelet-HLH	Firstorder	Kurtosis
eCTV20	wavelet-HHH	Firstorder	Skewness
eCTV20	wavelet-HHL	Gldm	DependenceNonUniformity
eCTV20	wavelet-HHL	Glcm	Imc1
sCTV5	wavelet-HLL	Glcm	InverseVariance
sCTV5	wavelet-HLL	Firstorder	Skewness
sCTV5	wavelet-LHL	Glszm	LargeAreaLowGrayLevelEmphasis
sCTV5	wavelet-LLH	Firstorder	Skewness
sCTV5	wavelet-HLH	Firstorder	Median
sCTV10	original	Glszm	LargeAreaHighGrayLevelEmphasis
sCTV10	wavelet-HLL	Glcm	InverseVariance
sCTV10	wavelet-LHH	Firstorder	Mean
sCTV10	wavelet-LLH	Gldm	SmallDependenceLowGrayLevelEmphasis
sCTV10	wavelet-HLH	Firstorder	Mean
sCTV10	wavelet-HHH	Gldm	SmallDependenceLowGrayLevelEmphasis
sCTV10	wavelet-HHH	Firstorder	Skewness
sCTV10	wavelet-HHL	Firstorder	Skewness
sCTV10	wavelet-HHL	Firstorder	Mean
sCTV10	wavelet-LLL	Gldm	SmallDependenceLowGrayLevelEmphasis
T2-weighted MRI image			
CTV	wavelet-HHH	Firstorder	Median
eCTV20	wavelet-HLL	Firstorder	Skewness
sCTV5	wavelet-HHH	Firstorder	Median
sCTV10	original	Gldm	SmallDependenceLowGrayLevelEmphasis

The prediction models with T1-weighted MRI images, T2-weighted MRI images, and the combination of T1and T2-weighted MRI images were evaluated. Figures 5—7 show the validation of the performance of the predictive models according to ROC metrics with 5-fold cross-validation. Table 5 shows the results of the accuracy, sensitivity, specificity, and AUC for the training and testing data.

Table 5
Assessment of the predictive performance of the predictive model for training and testing data with T1-weighted MRI image (T1), T2-weighted MRI image (T2), and the combination of T1- and T2-weighted MRI images (T1&T2).

	T1		**T2**		**T1&T2**	
	Training	Test	Training	Test	Training	Test
Sensitivity	89.9	86.4	87.8	87.4	97.6	93.1
Specificity	81.7	74.9	31.3	38.1	92.2	81.6
Accuracy	87.2	81.8	67.9	72.2	95.9	88.7
AUC		0.89		0.69		0.94

The average accuracy of the 5 models for the testing data was 81.8% with T1-weighted MRI image, 72.2% with T2-weighted MRI image, and 88.7% with a combination of T1- and T2-weighted MRI images. The average of the 5 models for the testing data was 0.89 with T1-weighted MRI image, 0.69 with T2-weighted MRI image, and 0.94% with a combination of T1- and T2-weighted MRI images. The prediction model with a combination of T1- and T2-weighted MRI images had higher accuracy and AUC. The prediction model with a T1-weighted MRI image had higher accuracy and AUC than the T2-weighted MRI image. Especially, the specificity of the prediction model with T2-weighted MRI images was under 40% for both training and testing data.

Discussion

Radiomics approach uses the image-based features as the imaging biomarker for the prediction of the grade of the tumor, treatment response, and side effects by treatment. The past studies (Ho et al, and Reuze et al) reported that the PET texture analysis could predict the recurrence of the cervix cancer than SUVmax [16, 17]. The AUC of the prediction model with PET texture analysis was 0.75 by Ho et al and 0.76 by Reuze et al Mengal et al improved the accuracy of the prediction of recurrence of advanced cervical cancer patients treated with concurrent chemoradiotherapy using the texture features extracted from T2-weighted MRI image and apparent diffusion coefficient (ADC) maps [18]. The AUC of the prediction model with the support vector machine was 0.89. Our study demonstrates the potential of radiomics analysis using T1- and T2-weighted MRI images to predict recurrence of cervix cancer after radiotherapy. The current study improved the accuracy by the prediction model of T1- and T2-weighted MRI images with the neural network. The PET is less clinically used than the MRI image and the MRI image had a more predictor.

Sun et al showed a potential of prediction of the clinical response to neoadjuvant chemotherapy with the radiomics analysis of combining the intratumoral and peritumoral regions on the pretreatment T1- and T2-weighted MRI images [19]. The current study investigated the usability of the radiomics model based on pretreatment T1- and T2-weighted MRI images for the prediction of recurrence after radiotherapy. The features of the segmentation of the shrink-CTV and extended-CTV in addition to the CTV were selected for the prediction model. The extended-CTV could extract the features

in and the boundaries of the tumor, which allows us to detect its associations with metastases within the microenvironment [20].

Nina et al investigated the correlation of the dynamic T1-weighted MRI image for the prediction of tumor control in patients treated with radiotherapy for advanced cervical cancer by pixel by pixel statistical analysis [21]. The dynamic MRI contrast enhancement can assess the regional variation in tumor microcirculation and allow for better assessment of low perfusion regions within tumors. They revealed the correlation of the poor blood supply and hypoxia contribute to radiation therapy failure.

The current study performed the radiomics analysis with T1- and T2-weighted MRI images, not the dynamic MRI contrast enhancement image. The shrink-CTV was mostly limited to the primary tumor region. In the shrink-CTV, the distribution of small dependence with lower pixel values was larger with T1-weighted MRI image and smaller with T2-weighted MRI image. It can suggest that the central tumor region is low blood flow. Thus, the radiomics feature can detect the hypoxia region by poor blood supply without dynamic contras enhanced MRI image. Although in the future, it is needed to validate the correlation of these features and blood flow and hypoxia, we think that the results of this study focused on T1-weighted MRI images are of great significance.

There were several limitations in the current study. The current study was conducted at a single institution with a limited number of cervix cancer patients. We consider it necessary to examine universal prediction model with a large number of cases in a multicenter. The current study used multiple MRI devices. A further study will be performed to reveal the robustness of the radiomics features between these devices. The prediction model was proposed with only pretreatment MRI images. Meng et al improved the prediction of the recurrence for cervix cancer using MRI images during treatment [22]. The changes in radiomics features from pretreatment and during treatment, called delta-radiomics features, have been investigated for their prognostic potential in cancer [23—25].

In the future, we reveal the correlation of the radiomics feature and the biological effect and construct a high versatile predictive model.

Conclusion

The radiomics analysis with T1- and T2-weighted MRI images could highly predict the recurrence of the cervix cancer after radiotherapy. The variation of the distribution and the difference of the pixel number at the peripheral and the center were important predictors.

Declarations

Acknowledgements

We gratefully acknowledge The Mathworks, Inc. for providing technical support.

CONFLICT OF INTEREST

The authors state that there are no conflicts of interest.

AUTHOR CONTRIBUTIONS

DK and IN are equally-contributed first author. DK and IN conceived and designed the study, and write the manuscript. DK, IN, MK, and YT performed data collection, data analysis and interpretation of results. IK, KT, MS, HT, YK and YN helped interpret the data and write the manuscript.

References

1. Siegel R.L. Miller K.D. Jemal A. Cancer statistics, 2019. CA Cancer J Clin. 2019; 69: 7-34.
2. Jemal, A. et al. Global cancer statistics. CA Cancer J Clin. 2011; 61: 69–90.
3. Sala E, Wakely S, Senior E, Lomas D. MRI of malignant neoplasms of the uterine corpus and cervix. AJR Am J Roentgenol. 2007; 188: 1577–87.
4. Zhenyu Liu , Yinyan Wang , Xing Liu, et al. Radiomics analysis allows for precise prediction of epilepsy in patients with low-grade gliomas. Neuroimage Clin, 2018; 19: 271-278.
5. J. Guo, Z. Liu, C. Shen, et al. MR-based radiomics signature in differentiating ocular adnexal lymphoma from idiopathic orbital inflammation Eur Radiol, 2018; 28: 3872-3881.
6. C. Shen, Z. Liu, Z. Wang, J, et al. Building CT radiomics based nomogram for preoperative esophageal cancer patients lymph node metastasis prediction Transl Oncol, 2018: 11: 815-824.
7. Lovinfosse P, Janvary ZL, Coucke P, Jet al. FDG PET/CT texture analysis for predicting the outcome of lung cancer treated by stereotactic body radiation therapy. Eur J Nucl Med Mol Imaging. 2016; 43: 1453–60.
8. Reuzé S, Orlhac F, Chargari C, et al. Prediction of cervical cancer recurrence using textural features extracted from 18F-FDG PET images acquired with different scanners. Oncotarget. 2017; 8(26): 43169-43179.
9. Meng J, Liu S, Zhu L, Zhu L, Wang H, Xie L, et al. Texture analysis as imaging biomarker for recurrence in advanced cervical cancer treated with CCRT. Sci Rep. 2018; 8: 11399.
10. Xie C, Yang P, Zhang X, et al. Sub-region based radiomics analysis for survival prediction in oesophageal tumours treated by definitive concurrent chemoradiotherapy. EBioMedicine. 2019; 44: 289–297.
11. Collins GS, Reitsma JB, Altman DG, et al. Transparent reporting of a multivariable prediction model for indi-vidual prognosis or diagnosis (TRIPOD): The TRIPOD statement. Ann. Intern. Med. 2015; 162: 55–63.
12. Fedorov A, Beichel R, Kalpathy-Cramer J, et al. 3D slicer as an image computing platform for the quantitative imaging network. Magn Reson Imaging. 2012;30:1323–1341.
13. Jjm VG, Fedorov A, Parmar C, et al. Computational Radiomics system to decode the radiographic phenotype. Cancer Res. 2017; 77: e104.
14. T ibshirani R. Regression shrinkage and selection via the lasso: a retrospective. J R Stat Soc Series B Stat Methodol. 2011;73:273–82.
15. J.X. Zhang, W. Song, Z.H. Chen, et al. Prognostic and predictive value of a microRNA signature in stage II colon cancer: a microRNA expression analysis. Lancet Oncol. 2013; 14(13): 1295-306.
16. Ho, K. C. et al. A preliminary investigation into textural features of intratumoral metabolic heterogeneity in (18)F-FDG PET for overall survival prognosis in patients with bulky cervical cancer treated with definitive concurrent chemoradiotherapy. Am J Nucl Med Mol Imaging 2016; 6(3): 166–175.
17. Reuzé S, Orlhac F, Chargari C, et al. Prediction of cervical cancer recurrence using textural features extracted from 18F-FDG PET images acquired with different scanners. Oncotarget. 2017; 8(26): 43169-43179.
18. Meng J, Liu SL, Zhu LJ, et al. Texture Analysis as Imaging Biomarker for recurrence in advanced cervical cancer treated with CCRT. Sci Rep. 2018; 8(1): 11399.
19. Sun C, Tian X, Liu Z, et al. Radiomic analysis for pretreatment prediction of response to neoadjuvant chemotherapy in locally advanced cervical cancer: a multicentre study. EBioMedicine. 2019; 46: 160-169.
20. Pei N, Guangjie Y, Jian G, et al. A CT-based radiomics nomogram for differentiation of focal nodular hyperplasia from hepatocellular carcinoma in the non-cirrhotic liver. Cancer Imaging. 2020; 20: 20.
21. Nina A. Mayr, William T.C. Yuh, Jeffrey C, et al. Pixel analysis of MR perfusion imaging in predicting radiation therapy outcome in cervical cancer. J Magn Reson Imaging. 2000; 12(6): 1027-33.

22. Meng J, Liu S, Zhu L, Zhu L, Wang H, Xie L, et al. Texture analysis as imaging biomarker for recurrence in advanced cervical cancer treated with CCRT. Sci Rep. 2018; 8: 11399.
23. Rao, S. X. et al. CT texture analysis in colorectal liver metastases: A better way than size and volume measurements to assess response to chemotherapy? United Eur. Gastroenterol. J. 2016; 4: 257–263.
24. Goh, V. et al. Assessment of response to tyrosine kinase inhibitors in metastatic renal cell cancer: CT texture as a predictive biomarker. Radiology. 2011; 261: 165–171.
25. Cunliffe, A. et al. Lung texture in serial thoracic computed tomography scans: Correlation of radiomics-based features with radiation therapy dose and radiation pneumonitis development. Int. J. Radiat. Oncol. Biol. Phys. 2015; 91: 1048–1056.

Figures

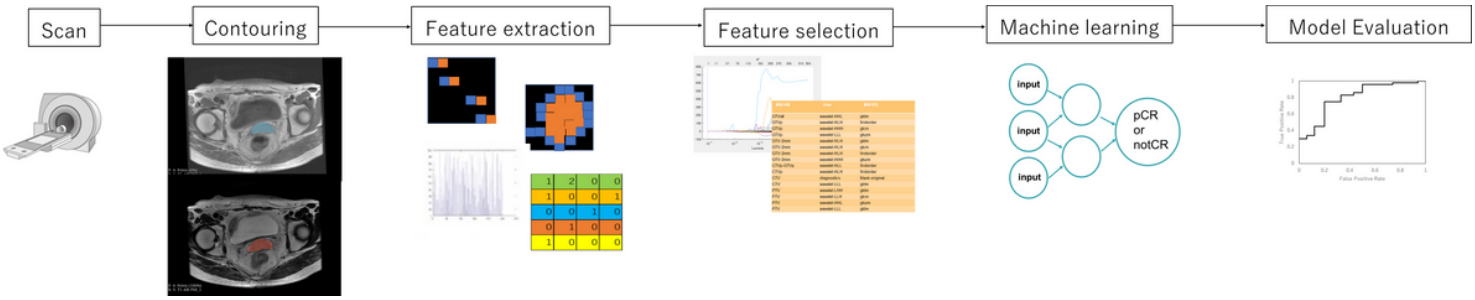

Figure 1

The process of the prediction model with radiomics analysis and machine learning.

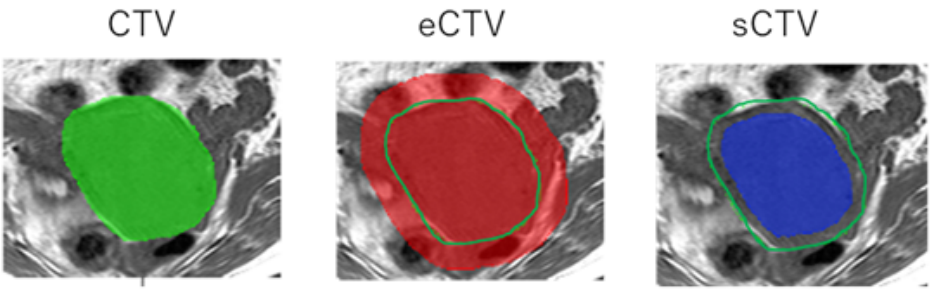

Figure 2

An example of the segmentation of CTV, extended-CTV (eCTV), and shrink-CTV (sCTV).

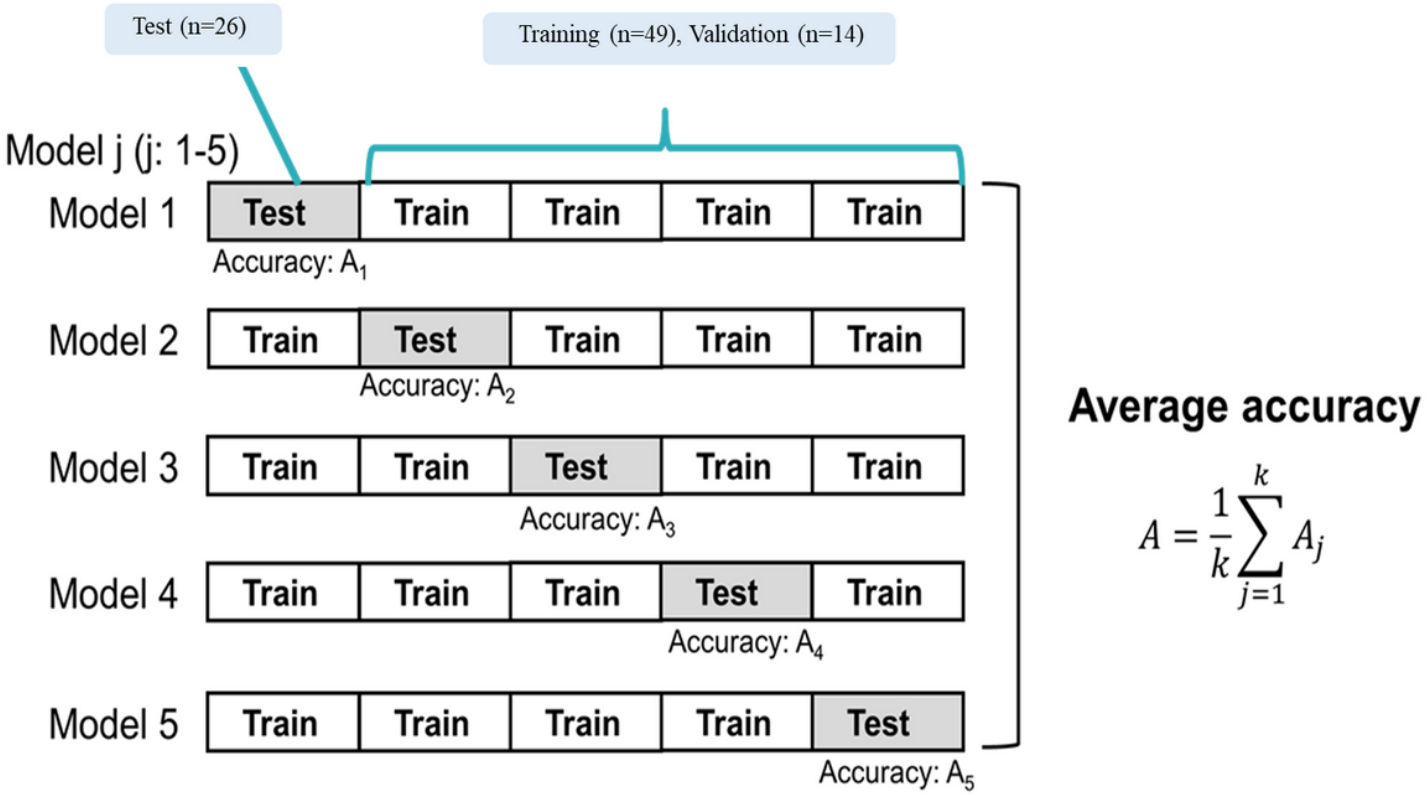

Figure 3

Training and testing with 5-fold cross-validation.

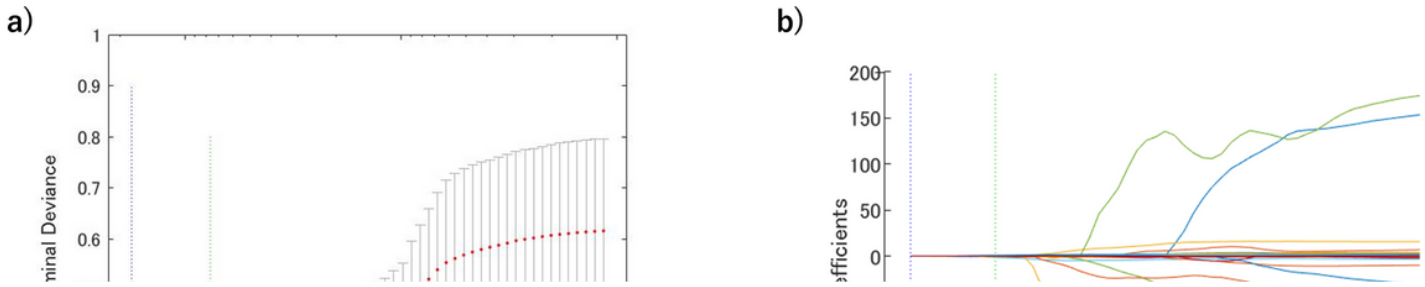

Figure 4

Radiomics features were selected using the LASSO regression. a) Tuning penalization parameter (λ) and minimum criterion in the LASSO model. The binomial deviance was plotted against log(λ). b) LASSO coefficient profiles of the 4185 radiomics features. The green line showed the optimal lambda in the LASSO analysis with the least partial likelihood deviance.

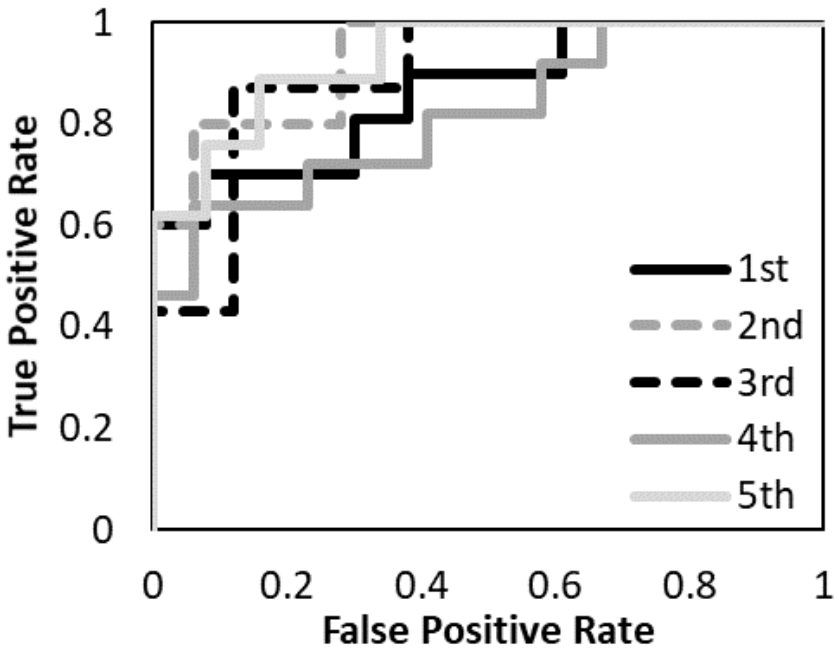

Figure 5

The performance of the predictive model with the T1-weighted MRI image was evaluated according to the ROC metrics.

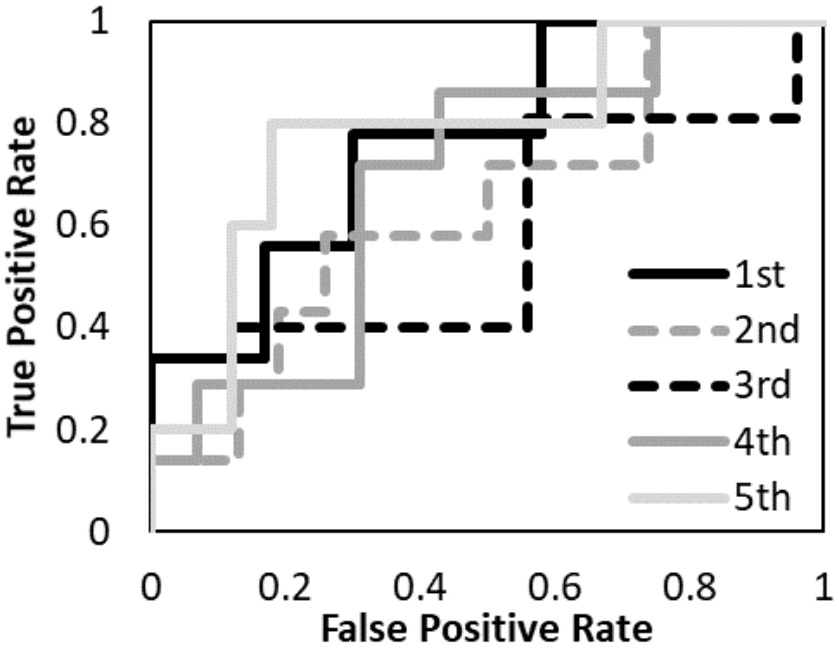

Figure 6

The performance of the predictive model with the T2-weighted MRI image was evaluated according to the ROC metrics.

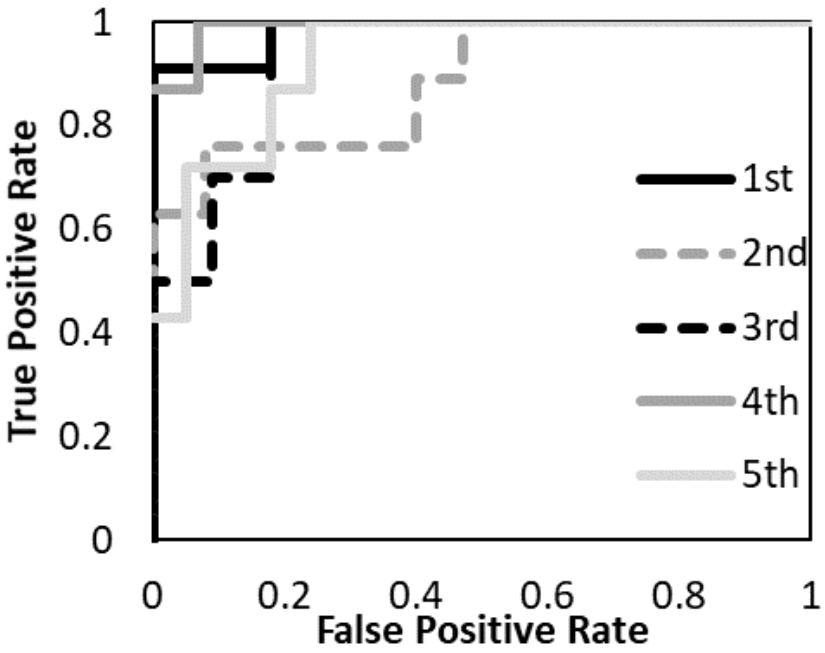

Figure 7

The performance of the predictive model with T1- and T2- weighted MRI images was evaluated according to the ROC metrics.

Supplementary Files

This is a list of supplementary files associated with this preprint. Click to download.

- SuplementalTable20211105.docx